Gauss-Kronrod Integration for rectangular closed conduits

P. Gruber[1], T. Staubli[2], F. Fahrni[2]

[1]*pgconsult, Grenzacherweg 116, 4125 Riehen, Switzerland*
[2]*HSLU Lucerne, Technikumstasse21, 6048 Horw, Switzerland*
E-mail (corresponding author): peter.gruber@hslu.ch

Abstract

There exist cases of closed conduits applications, where the performance of the chosen configuration of the ATT flow measurement is unsatisfactory. One method of improving the situation is to add more paths to the existing installations In case of circular closed conduits and Gauss-Jacobi integration, there exists the nice feature, that by interlacing new paths in between the old paths, the positions of the old paths do not change without losing in accuracy of the discharge calculation. That means that polynomial deviations from the assumed weighting function $W=(1-x^2)^{1/2}$, of order $2(2N^*+1)-1 = 4N^*+1$ (equal the degree of exactness of the quadrature formula) can be integrated without error. N* corresponds to the number of original paths. In case of an original 4-path in one plane configuration extended to a 9-path in one plane configuration, N*=4, N=9, degree of exactness=17. This has an enormous advantage, because the already implemented path positions do not have to be changed. In case of rectangular closed conduits, this is unfortunately no more the case. For the optimal interlacing arrangement, all positions change. For rectangular conduits, in theory the positioning is less of a problem due to the fact, that all the transducers have the same pill angle independent on the transducer positions. Nevertheless, from the installation effort point of view, it is often a request to not move the old positions. Kronrod [1] derived optimal formulas for the interlacing positions and all weights under the constraints of the old N* positions. Due to the constraints, the degree of the quadrature formula is 3N*+1 (N* even, e.g. N*=4, degree=13) or 3N*+2 (N* odd). The paper gives the corresponding positions and weights for the interesting cases N*=2, 3 and 4, and compares the results with the known choice of positions and weights for assumed and simulated flow profiles. As the flow profiles are in reality not rational functions, the loss in polynomial accuracy is not always clear.

1. Introduction

The performance of an ATT flow measurement installation is in applications, where the hydraulic situation is difficult or not well known, hard to evaluate. In recent years, improved CFD flow simulations for hydraulic difficult situations allow a reasonable estimate of the integration error of the measurement. The question of measurement location, orientation and path configuration (number of layers, crossed, not crossed) are important parameters that can be varied for finding an optimal solution by CFD simulations. Figure 1 shows two examples of crossed 8-path configurations (2 vertical planes and 4 layers each)

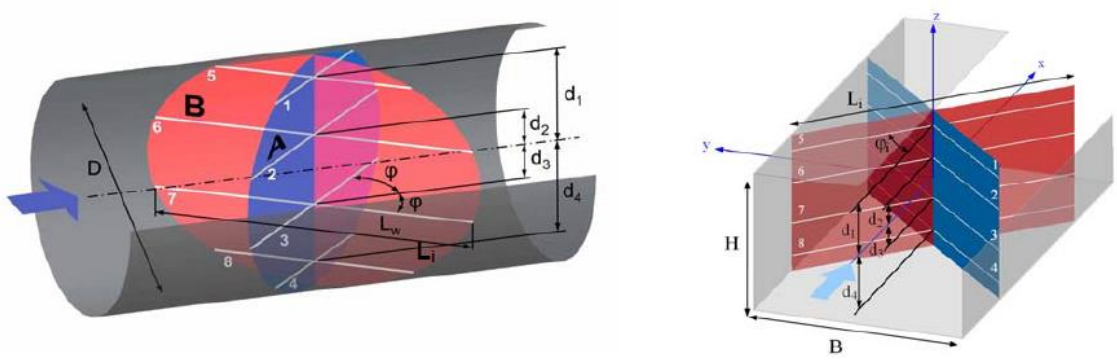

Fig. 1: Crossed path configuration for the ATT measurement method

After CFD simulation studies or from experience of experts, the measurement is finally parametrized. A common example is the 8-path (2 times 4 paths in 2 planes) configurations with Gauss-Jacobi positions and weightings for circular closed conduits. After the installation, commissioning and putting into operation of such a measurement, the individual path velocities respectively axial and transverse velocities, are recorded and monitored. If unusual profiles are observed and installation errors can be excluded, one way to improve the accuracy of the flow measurement is increasing the number of paths. Marushchenko, Gruber [2] showed that with an increase from 4 paths to 5 paths (centre path) in one plane, substantial improvements can be achieved. The future revised version of IEC60041 standard [3] will open up the number of paths up

to 10(20). The ASME PTC18 code is proposing for difficult hydraulic situations to implement 9 (18) paths [4]. The improvement by adding more paths suffers of course from the law of diminishing returns, which states that the gain in accuracy is decreasing with each additional path.
The case of interlacing additional paths is particularly interesting for circular sections because the positions of the old positions do not change, as is shown in section 2. For rectangular sections, similar arguments for the accuracy hold as in the case of circular sections. The positioning however is different for all paths. It must be noted, that in case of rectangular sections, a repositioning of the old path positions is not a problem from the transducers (pill angles) perspectives. We consider here however the situation that a repositioning is not an option. Reasons for this could be the following:

- Transducers are difficult to remove from old positions
- Remounting of transducers is costly due to difficult access
- New transducer positions not accessible

2. Existing tables for positions and weights

2.1 Original table
In 2010, Tresch & al [5] presented the derivation of general positions (see Figure 1 & 2) and weights and the following Table 1 with positions and weights for four different cases

	Gauss-Jacobi p &w		**OWICS p &w**		**Gauss-Legendre p & w**		**OWIRS p & w**	
Number of paths N	Positions $d_i/(D/2)$	Weights w_i	Positions $d_i/(D/2)$	Weights w_i	Positions $d_i/(D/2)$	Weights w_i	Positions $d_i/(D/2)$	Weights w_i
1	0	1.570796	0	1.513365	0	2	0	1.837286
2	0.5	0.906900	0.487950	0.890786	0.577350	1	0.550482	0.969761
3	0	0.785398	0	0.768693	0	0.888889	0	0.853688
	0.707107	0.555360	0.695608	0.553707	0.774597	0.555556	0.752355	0.557403
4	0.309017	0.597566	0.303783	0.588228	0.339981	0.652145	0.329729	0.634200
	0.809017	0.369316	0.799639	0.371884	0.861136	0.347855	0.844510	0.356143
5	0	0.523599	0	0.515768	0	0.568889	0	0.554092
	0.5	0.453450	0.493266	0.448857	0.538469	0.478629	0.525989	0.470657
	0.866025	0.261799	0.858534	0.265433	0.906180	0.236927	0.893646	0.245772
6	0.222521	0.437547	0.219676	0.432160	0.238619	0.467914	0.233427	0.458140
	0.623490	0.350885	0.616712	0.348913	0.661209	0.360762	0.649158	0.357811
	0.900969	0.194727	0.894939	0.198413	0.932470	0.171324	0.922789	0.179346
7	0	0.392699	0	0.388174	0	0.417959	0	0.409876
	0.382683	0.362807	0.378515	0.359341	0.405845	0.381830	0.398454	0.375801
	0.707107	0.277680	0.700797	0.277122	0.741531	0.279705	0.730661	0.279255
	0.923880	0.150279	0.918958	0.153701	0.949108	0.129485	0.941444	0.136455
8	0.173648	0.343763	0.171873	0.340324	0.183435	0.362684	0.180326	0.356680
	0.5	0.302300	0.495335	0.300163	0.525532	0.313707	0.517455	0.310151
	0.766044	0.224375	0.760344	0.224578	0.796666	0.222381	0.787085	0.223172
	0.939693	0.119388	0.935615	0.122463	0.960290	0.101229	0.954089	0.107221
9	0	0.314236	0	0.311216	0	0.330239	0	0.325159
	0.309017	0.298715	0.306222	0.296281	0.324253	0.312347	0.319446	0.308080
	0.587785	0.254205	0.583053	0.252911	0.613371	0.260611	0.605335	0.258640
	0.809017	0.184635	0.803925	0.185265	0.836031	0.180648	0.827640	0.182040
	0.951057	0.097090	0.947631	0.099815	0.968160	0.081274	0.963048	0.086431

Table 1: general table for position & weights for variable number of paths in one plane

The table is based on the original Gaussian quadrature method with an additional weighting function *W(z)*. In this application of the method, the area flow function (AFF) *F(z)* corresponds to the weighting function *W(z)*.
F(z) describes the distribution of the partial flow rates for each height *z* and is expressed by the product between the averaged axial velocity and the width *b(z)* of the conduit at height *z* (Staubli & al [5])

$$F(z) = \bar{v}_{ax}(z) \cdot b(z)\ [m^2/s] \tag{1}$$

At the height of the path position z_i, the width $b(z_i)$ is equal to the projected path length $L_{i,proj}$:

$$b(z_i) = L_{i,proj} = L_i \cdot \sin(\varphi) \tag{2}$$

Integration of *F(z)* over the whole cross section yields the discharge *Q*

$$Q = \int_{-\frac{D}{2}}^{\frac{D}{2}} F(z)dz \tag{3}$$

The different integration weights of the Gauss-Jacobi and the OWICS method for circular section and Gauss-Legendre and OWIRS methods have their origin in different assumption on the shape of the theoretical reference area flow function respectively velocity distribution. They can be distinguished by a single parameter κ. The assumed AFF is therefore given by

$$F_{ref}(z) = C \cdot \left(1 - \frac{z^2}{\left(\frac{D}{2}\right)^2}\right)^{\kappa} \left[\frac{m^2}{s}\right] \tag{4}$$

C: case dependent constant

Parameter κ for circular sections:	Gauss-Jacobi (GJ):	0.5	OWICS: 0.6
Parameter κ for rectangular sections:	Gauss-Legendre (GL):	0	OWIRS: 0.15

With the normalization $\zeta = \frac{z}{D/2}$, F_{ref} can be written as:

$$F_{ref}(z) = C \cdot (1 - \zeta^2)^{\kappa} \left[\frac{m^2}{s}\right] \tag{5}$$

With this assumed AFF F_{ref} and the proper choice of κ, the positions and weights w_i of Table 1 can be determined by the Gaussian quadrature.

The discharge *Q* can then be computed by:

$$Q = \frac{D}{2} \cdot \sum_{i=1}^{N} w_i \cdot \bar{v}_{ax}(z_i) \cdot b(z_i) \tag{6}$$

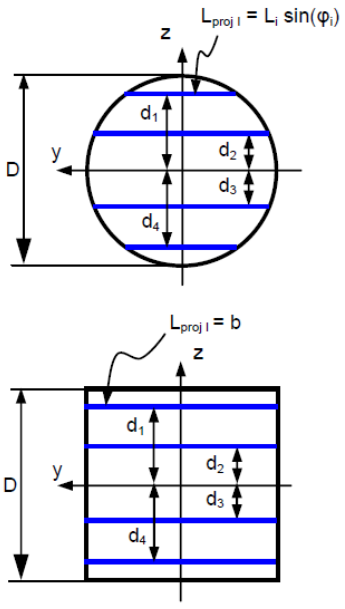

Fig. 2: path positions

2.2 IEC 60041 table

If the complete OWICS or OWIRS methods are used, all positions and weights are always different for the Gauss-Jacobi and the Gauss-Legendre cases as can be seen from Table 1. The existing IEC 60041standard demands that a 4-path (1 plane) or 8 path (2 crossed planes) installation has to use Gauss-Jacobi or Gauss-Legendre positions for the path heights. This means that the pill angles of the transducers for circular sections are designed specifically for the Gauss-Jacobi positions. Most transducers in IEC conformal installations have therefore been mounted in this way in the past. That is the reason why the OWICS/OWIRS methods were modified in such a way that the OWICS/OWIRS weights are determined for the Gauss-Jacobi rep. Gauss-Legendre positions (Table 3 cases 2 & 4). Table 3 shows additionally an augmented table (number of paths from 1 to 10 in one plane). For IEC conformal installations the number N of paths in one plane is not foreseen for N<4. Additionally, if the actual positions of an installation are measured after mounting the transducers, the weights should be recalculated with the actual positions. An uncertainty analysis for mispositioning the OWICS/OWIRS positions shows that the induced error by the proposed procedure is very small [6], [7].

	Gauss-Jacobi positions & Gauss-Jacobi weights		**Gauss-Jacobi positions & OWICS weights**		**Gauss-Legendre positions & Gauss-Legendre weights**		**Gauss-Legendre positions & OWIRS weights**	
Number of paths N	Positions $d_i/(D/2)$	Weights w_i	Positions $d_i/(D/2)$	Weights w_i	Positions $d_i/(D/2)$	Weights w_i	Positions $d_i/(D/2)$	Weights w_i
1	0	1.570796	0	1.513365	0	2	0	1.837286
2	0.5	0.906900	0.5	0.899243	0.577350	1	0.577350	0.959152
3	0	0.785398	0	0.792715	0	0.888889	0	0.909365
	0.707107	0.555360	0.707107	0.546150	0.774597	0.555556	0.774597	0.532319
4	0.309017	0.597566	0.309017	0.598640	0.339981	0.652145	0.339981	0.655527
	0.809017	0.369316	0.809017	0.365222	0.861136	0.347855	0.861136	0.336984
5	0	0.523599	0	0.521504	0	0.568889	0	0.562705
	0.5	0.453450	0.5	0.455836	0.538469	0.478629	0.538469	0.485402
	0.866025	0.261799	0.866025	0.258135	0.906180	0.236927	0.906180	0.228094
6	0.222521	0.437547	0.222521	0.437269	0.238619	0.467914	0.238619	0.467005
	0.623490	0.350885	0.623490	0.351849	0.661209	0.360762	0.661209	0.363690
	0.900969	0.194727	0.900969	0.192460	0.932470	0.171324	0.932470	0.165695
7	0	0.392699	0	0.393562	0	0.417959	0	0.420611
	0.382683	0.362807	0.382683	0.361873	0.405845	0.381830	0.405845	0.379019
	0.707107	0.277680	0.707107	0.278885	0.741531	0.279705	0.741531	0.283085
	0.923880	0.150279	0.923880	0.148296	0.949108	0.129485	0.949108	0.124840
8	0.173648	0.343763	0.173648	0.343866	0.183435	0.362684	0.183435	0.363020
	0.5	0.302300	0.5	0.301961	0.525532	0.313707	0.525532	0.312642
	0.766044	0.224375	0.766044	0.225064	0.796666	0.222381	0.796666	0.224377
	0.939693	0.119388	0.939693	0.117966	0.960290	0.101229	0.960290	0.097845
9	0	0.314236	0	0.313796	0	0.330239	0	0.328802
	0.309017	0.298715	0.309017	0.299176	0.324253	0.312347	0.324253	0.313833
	0.587785	0.254205	0.587785	0.253670	0.613371	0.260611	0.613371	0.258953
	0.809017	0.184635	0.809017	0.185362	0.836031	0.180648	0.836031	0.182700
	0.951057	0.097090	0.951057	0.095849	0.968160	0.081274	0.968160	0.078403
10	0.142315	0.282716	0.142315	0.282666	0.148874	0.295520	0.148874	0.295355
	0.415415	0.259734	0.415415	0.259886	0.433395	0.269269	0.433395	0.269783
	0.654861	0.215901	0.654861	0.215622	0.679410	0.219085	0.679410	0.218183
	0.841254	0.154364	0.841254	0.154852	0.865063	0.149453	0.865063	0.150878
	0.959493	0.080483	0.959493	0.079523	0.973907	0.066671	0.973907	0.064413

Table 2: augmented table for positions and weights proposed for IEC 60041 revision,

3. Adding interlacing positions and weights: Gauss-Kronrod

The Gauss–Kronrod quadrature formula is an adaptive method for numerical integration. It is a variant of Gaussian quadrature, in which the evaluation points are chosen such that an accurate approximation can be computed by re-using the information produced by the computation of a less accurate approximation. It is an example of what is called a nested quadrature rule: for the same set of function evaluation points, it has two quadrature rules, one higher order and one lower order (the latter called an embedded rule). The difference between these two approximations is used to estimate the calculational error of the integration. The formulae are named after Alexander Kronrod [1], who derived them in the 1960s, and Gauss. Gauss–Kronrod quadrature is used in the QUADPACK library, the GNU Scientific Library, the NAG Numerical Libraries and R [5].

The original Gaussian N quadrature rule for the approximation of the integral of a function f with a weight function W is given for an interval [-1, 1] by the following formula:

$$\int_{-1}^{1} W(\zeta) f(\zeta) d\zeta = \sum_{i=1}^{N} w_i f(\zeta_i) + R_N^G(f) \tag{7}$$

ζ_i and w_i are the positions and the positive weights which can be determined such that the degree of exactness is [9]

$$d_N^G = 2N - 1 \tag{8}$$

That means that a polynomial function f of order 2N-1 can be integrated by the weighted sum of equation (7) without error:

$$R_N^G(f) = 0 \tag{9}$$

Polynomial function of higher order or transcendental functions can only integrated with a remaining error term. With increasing the number N, the approximation of equation (7) gets better for transcendental functions.
The position and weights w_i and ζ_i, i=1,…N are the ones listed in Table 1 for four different kind of weight function *W*, where only the nonnegative positions are listed due to the fact that the positions are symmetrical to the ζ-axis.

The Gauss-Kronrod quadrature formula, extending equation (7), has the form [9]

$$\int_{-1}^{1} W(\zeta) f(\zeta) d\zeta = \sum_{i=1}^{N^*} w_i^* f(\zeta_i) + \sum_{l=1}^{N^*+1} w_l^* f(\zeta_l) + R_{N^*}^K(f) \tag{10}$$

Equation (10) means that the approximation of the integration is as follows: At the N* old positions ζ_i, i=1,…N*, the N* weights w_i^* are newly computed. The old function values $f(\zeta_i)$ are then added up weighted by w_i^*. The second sum considers the N*+1 new interlacing positions ζ_l, *l*=1,…,N*+1. Kronrod derived the new positions ζ_l, *l*=1,…,N*+1 and the new weights w_i^*, i=1,…,N* and w_l^*, *l*=1,…,N*+1, such that despite the constraints of keeping the old positions fixed the degree of exactness is

$$d_N^K = 3N^* + 1 \qquad \text{for N* even}$$

$$d_N^K = 3N^* + 2 \qquad \text{for N* odd} \tag{11}$$

In case of an odd N* one degree can be gained because the centre position 0 is not changed. If we compare this exactness with the one of the pure Gaussian quadrature formula where all N=2N*+1 positions and the corresponding weights are determined, a reduction of exactness of

$$\Delta d_N^K = d_N^G - d_N^K = 2(2N^* + 1) - 1 - (3N^* + 1) = N^* \qquad \text{for N* even}$$

$$\Delta d_N^K = d_N^G - d_N^K = 2(2N^* + 1) - 1 - (3N^* + 2) = N^* - 1 \qquad \text{for N* odd} \tag{12}$$

is inevitable.

For the interesting cases in for ATT applications, the following table results

N*	d_N^G	d_N^K	Δd_N^K	
2	9	7	2	2 to 5 paths
3	13	11	2	3 to 7 paths
4	17	13	4	4 to 9 paths

Table 3: loss of exactness for the a general weight function W and Gauss-Kronrod quadrature

3.1 Special case: Jacobi-Chebyshev weight functions and interlacing nods
The Jacobi weight function is defined as

$$W^{(\alpha,\beta)}(\zeta) = (1-\zeta)^{\alpha}(1+\zeta)^{\beta} \qquad \text{on [-1,1]} \qquad \alpha > -1, \beta > -1 \qquad (13)$$

Special cases are the four Chebyshev weights if $|\alpha| = |\beta| = \frac{1}{2}$, as for each one of them the corresponding Gauss-Kronrod formula has a special form with explicitly known nodes and weights [9]. For the Chebyshev weight of the second kind with $\alpha = \beta = \frac{1}{2}$,

$$W^{(0.5,0.5)}(\zeta) = (1-\zeta^2)^{0.5} \qquad (14)$$

which corresponds to the AFF for κ=0.5 of equation (5). It turns out that for this case the Gauss-Kronrod formula is the the N=2N*+1 Gauss-Jacobi formula for this weight. Therefore, in case of circular closed conduits and Gauss-Jacobi integration, there exists the nice feature, that by interlacing N*+1 new paths in between the old N* paths to total of N=2N*+1 paths (e.g. N*=4, 2N*+1=9), the positions of the old paths do not change without losing in accuracy [10]. That means, that polynomial deviations from the assumed weighting function $W^{(0.5,0.5)}(\zeta) = (1-\zeta^2)^{0.5}$ of order 2(2N*+1)-1 =4N*+1 (equal the degree of the quadrature formula, e.g. 17) can still be integrated without error. This has the additional benefit, that the already implemented path positions do not have to be changed. This can for instance be seen in Table 1 if one goes up in the case of Gauss-Jacobi from N=2 to N=5, the position 0.5 remains the same.

3.2 Kronrod position and weights
In case of rectangular section, the weighting function *W* is equal 1, and the nice property of section 3.1 does no more hold. Therefore the loss in exactness given by equations (12) has to be considered. The consequence of this is, that for polynomial functions the Gauss-Kronrod approximation is slightly inferior to the original Gauss-Legendre approximation. For transcendental function like log and exponential functions, the loss cannot be specified straightforward. Well developed turbulent flow profiles are often approximated by complicated transcendental and functions. For the three path configuration N=3,4 and 5 in one plane, Table 4 gives the Gauss-Kronrod positions and weights.

N=5		**N=7**		**N=9**	
$d_i/(D/2)$	w_i	$d_i/(D/2)$	w_i	$d_i/(D/2)$	w_i
0	0.622222	0	0.450917	0	0.346443
+/-0.577350	0.490909	+/-0.434244	0.401340	**+/-0.339981**	0.326919
+/-0.925820	0.197978	**+/-0.774597**	0.268488	+/-0.640286	0.266798
		+/-0.960491	0.104656	**+/-0.861136**	0.170054
				+/-0.976560	0.062978

Table 4: Kronrod positions & weights

The positions in bold figures indicate the Gauss-Legendre positions for the old path numbers N*=2, 3 and 4

3.3 Gauss-Legendre and OWIRS
In order to compare the performance of the Gauss-Kronrod approximation, the following approximations were applied to the same flow profiles in a rectangular cross section:

- Gauss-Legendre positions and weights
- OWIRS positions and weights
- Gauss-Legendre positions and OWIRS weights

Tables 5: positions and weights of above cases

N=5

Gauss-Legendre positions & weights		OWIRS positions & weights		Gauss- Legendre positions & OWIRS weights	
$d_i/(D/2)$	w_i	$d_i/(D/2)$	w_i	$d_i/(D/2)$	w_i
0	0.568889	0	0.554092	0	0.562705
+/-0.538469	0.478629	+/-0.525989	0.470657	+/-0.538469	0.485402
+/-0.906180	0.236927	+/-0.893646	0.245772	+/-0.906180	0.228094

N=7

Gauss-Legendre positions & weights		OWIRS positions & weights		Gauss- Legendre positions & OWIRS weights	
$d_i/(D/2)$	w_i	$d_i/(D/2)$	w_i	$d_i/(D/2)$	w_i
0	0.417959	0	0.409876	0	0.420611
+/-0.405845	0.381830	+/-0.398454	0.375801	+/-0.405845	0.379019
+/-0.741531	0.279705	+/-0.730661	0.279255	+/-0.741531	0.283085
+/-0.949108	0.129485	+/-0.941444	0.136455	+/-0.949108	0.124840

N=9 Gauss-Legendre positions & weights OWIRS positions & weights

Gauss-Legendre positions & weights		OWIRS positions & weights		Gauss- Legendre positions & OWIRS weights	
$d_i/(D/2)$	w_i	$d_i/(D/2)$	w_i	$d_i/(D/2)$	w_i
0	0.330239	0	0.325159	0	0.328802
+/-0.324253	0.312347	+/-0.319446	0.308080	+/-0.324253	0.313833
+/-0.613371	0.260611	+/-0.605335	0.258640	+/-0.613371	0.258953
+/-0.836031	0.180648	+/-0.827640	0.182040	+/-0.836031	0.182700
+/-0.968160	0.081274	+/-0.963048	0.086431	+/-0.968160	0.078403

3.4 Comparison of positions and weights

Figure 3 shows the difference of the positions and corresponding weights for all 4 approximations.

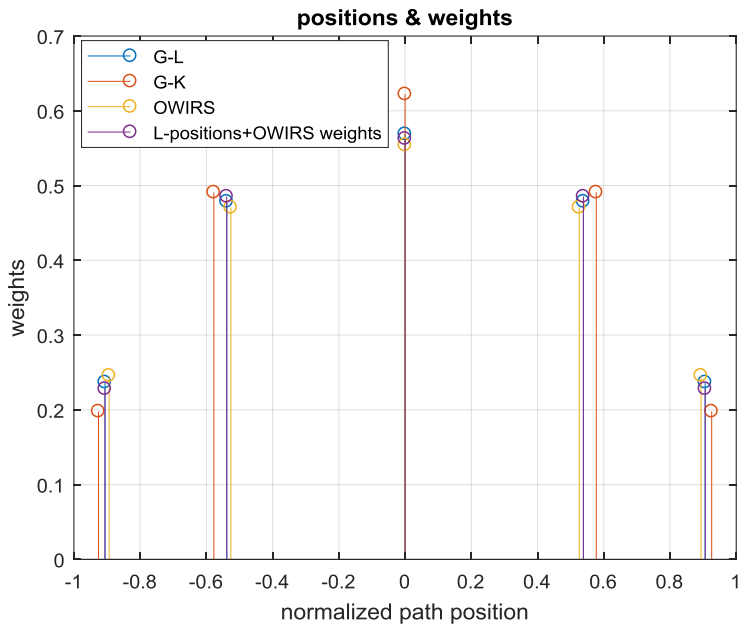

Fig. 3: path positions and weights for G-L (Gauss-Legendre), G-K (Gauss-Kronrod), OWIRS and Legendre positions and OWIRS weights

4. Analytical examples

4.1 Polynomial profiles

The theory is first checked with polynomial velocity profiles of increasing order. The choice should reflect in some way possible profiles in reality. The restrictions to the profile is that on the two boundaries it should be zero, always positive and the number of local maxima at most two. The choice of the polynomials is of the following form:

$$p(\zeta) = (1-\zeta^2)(1+b_1\zeta)(1+a_1\zeta+a_2\zeta^2+a_3\zeta^3+a_4\zeta^4+a_5\zeta^5)^2 \quad (15)$$

With b_1=0.2 and five different choices of a_i:

	a_1	a_2	a_3	a_4	a_5
3rd order	0	0	0	0	0
7th order	0	0.7813	0	0	0
9th order	0	0.7813	0.3	0	0
11th order	0	0.7813	0.3	0.1	0
13th order	0	0.7813	0.3	0.1	-0.2

Table 6:chosen polynoms of different orders

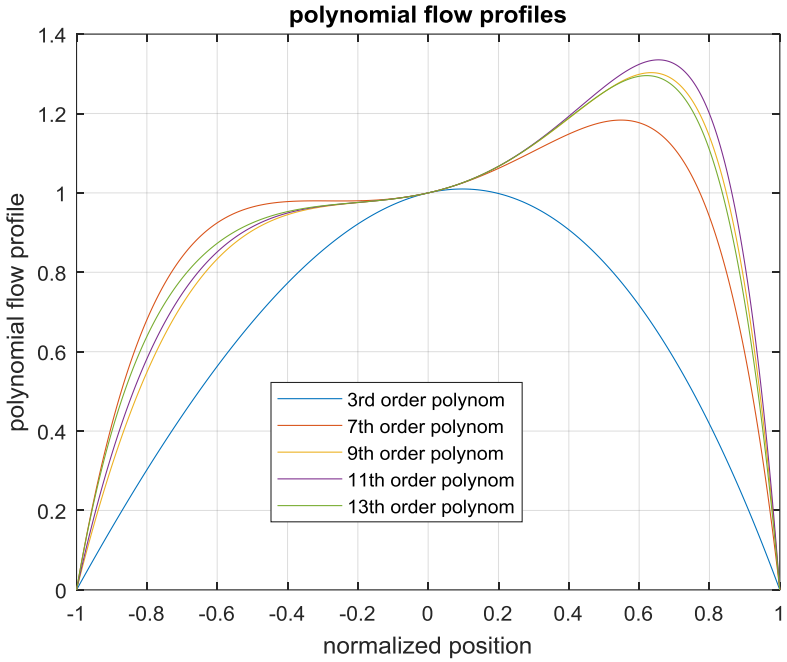

Fig. 4: graph of chosen polynomials

The test is carried out with the approximation order of N=5.

Polynomial order	Exact integral I_{ref}	Gauss-Legendre	Gauss-Kronrod	G-L position OWIRS weights	OWIRS
3rd order	1.33333333	1.33331421	1.33331447	1.33358938	1.33395010
7th order	1.81975446	1.81973431	1.81973284	1.81950717	1.82215809
9th order	1.84513542	1.84511532	1.84444705	1.84445123	1.84790271
11th order	1.87880208	1.87884657	1.87750735	1.87765137	1.88205810
13th order	1.86605409	1.86691547	1.86659504	1.86605409	1.86985859

Table 6: Discharge measurement of the four cases for the five polynoms

The integration error is computed according to

$$\epsilon = \frac{I - I_{ref}}{I_{ref}} 100\% \qquad (16)$$

Errror ε in %	Exact integral	Gauss-Legendre	Gauss-Kronrod	G-L position OWIRS weights	OWIRS
3rd order	0	**-0.0014**	**-0.0014**	0.0192	0.0463
7th order	0	**-0.0011**	**-0.0012**	-0.0136	0.1321
9th order	0	**-0.0011**	-0.0373	-0.0371	0.1500
11th order	0	0.0024	-0.0689	-0.0612	0.1733
13th order	0	-0.0176	-0.0348	-0.0637	0.1400

Table 7: errors of discharge measurements

Table 7 reflects the expected results in accuracy. The error numbers in bold belong to the cases where the theory tells that error zero is to be expected. Therefore errors of less 0.0015% are considered to be numerical errors. The following remarks can be made for the four cases:

- Gauss-Legendre: best performance. Up to 9th order polynomials, the error is zero. For higher order a slow increase of the error can be observed.
- Gauss-Kronrod: second best performance. Up to 7th order polynomials, the error is zero. For higher order, the error rises up to 2-3 times larger values as for the Gauss-Legendre case.
- G-L positions & OWIRS weights: Even for small order polynomials, the error is as high as for the G-L case for high order polynomials. With increasing order of the polynomials, the error is comparable to the Gauss-Kronrod case.
- OWIRS: The worst performance because the method is optimized for the OWIRS profile. For higher order polynomials, the error is ~constant (0.15%).

4.2 Exponential profiles

In order to check the performance of the methods, an artificial analytical profile was generated of the form:

$$F(x) = y_{max}(1 - \alpha e^{-\frac{x}{T_W}} - (1-\alpha)e^{-\frac{x}{T_i}}) \qquad x=[0,1] \qquad (17)$$

The four parameters are chosen, such that a realistic flow profile can be obtained, which is similar to the Gersten Herwig profile [11,12]. The maximal value and the value for the representative wall distance were defined accordingly. The inner exponential decay rate T_2, y_{max} and α were kept constant, while the wall exponential decay rate was varied between

T_W=[0.002 0.02 0.04 0.06 0.1];
T_2=0.1;
y_{max}=1.23;
α=0.81;

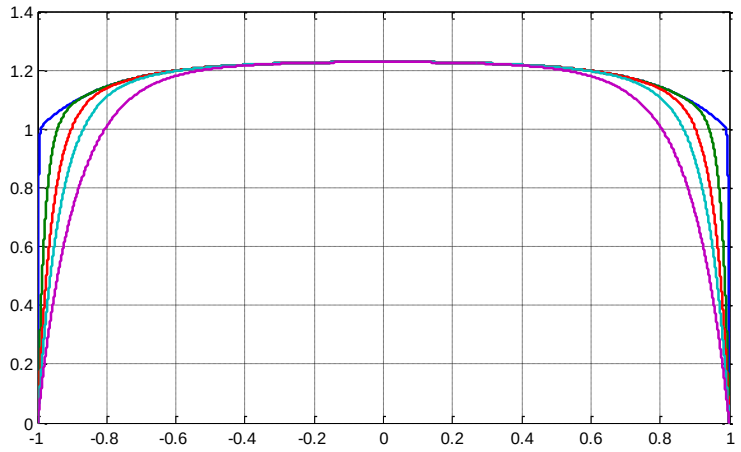

Fig. 5: exponential profiles, slowest rise corresponds to largest T_W

Again, the test is carried out with the approximation order of N=5.

	Exact integral I_{ref}	Gauss-Legendre	Gauss-Kronrod	G-L position OWIRS weights	OWIRS
T_W =0.002	2.3632	2.3676	2.3674	2.3572	2.3550
T_W =0.02	2.3273	2.3632	2.3578	2.3530	2.3526
T_W =0.04	2.2874	2.3223	2.3056	2.3136	2.3207
T_W =0.06	2.2476	2.2683	2.2520	2.2616	2.2714
T_W =0.1	2.1679	2.1733	2.1652	2.1697	2.1777

Table 8: Integral (discharge) of the four cases for five exponential profiles

Errror ε in %	Exact integral	Gauss-Legendre	Gauss-Kronrod	G-L position OWIRS weights	OWIRS
T_W =0.002	0	0.1863	0.1803	-0.2536	-0.3450
T_W =0.02	0	1.5441	1.3087	1.1043	1.0875
T_W =0.04	0	1.5246	0.7951	1.1438	1.4537
T_W =0.06	0	0.9201	0.1948	0.6212	1.0610
T_W =0.1	0	0.2507	-0.1239	0.0827	0.4520

Table 9: measurement error of the four cases for five exponential profiles, green: best, red: worst

For this profile, the following can be observed:

- Contrary to the polynomial profiles, this choice of exponential profiles never has Gauss-Legendre as winner. In two cases, Gauss-Legendre even shows the worst performance.
- Surprisingly enough, the Gauss-Kronrod approximation is in three out of 5 cases the best. The reason for these results is not yet clear. However, it seems to be that the interlacing positions in between the old Gauss-Legendre positions can better cope with the exponential behaviour of the profile.
- OWIRS behaves badly in 3 out of 5 cases. This is not surprising, as the OWIRS positions and weights are not optimized for an exponential profile.

5. CFD simulations

CFD simulations were carried out for two types of cross sections and three different flow velocities. The two cross sections are:

- Square shape with side length $a=b=1.4m$
- Rectangular shape with 1.5m width $a=1.5m$ and height $b=4.5m$.

The velocities v are chosen as 0.2m/s, 2m/s and 10m/s. This results for the Reynolds number

$$Re = v\frac{2ab}{a+b}10^6 \tag{18}$$

the following quantities:

Square: $Re = 0.28 * 10^6$ to $Re = 14 * 10^6$
Rectangle: $Re = 0.45 * 10^6$ to $Re = 22.5 * 10^6$

The simulated square cross section is shown in Figure 6. For the rectangular cross section the length of the conduit is also 6m.

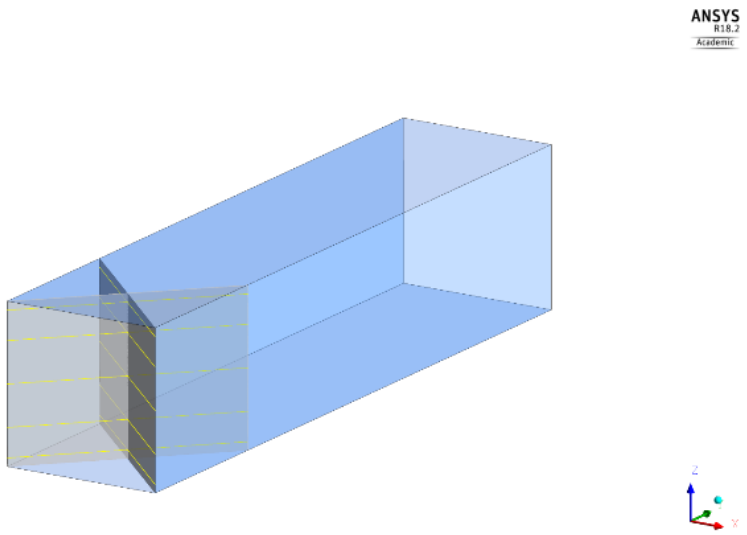

Fig. 6: simulated square cross section, 1.4m x 1.4m x 6m, 2E10P (two planes with five paths in each plane)

Figure 7 shows contour plot of the axial velocity (x-axis) for the square cross section. It is clearly visible that at the centre of the square the maximal velocity is attained. Figure 8 visualizes the secondary flow components. For each simulated

cell a normalized vector shows the direction of the flow. As the number of cells along the boundaries is much higher, the concentration of vectors along the boundaries is also higher. The absolute value of the secondary flow was very small.

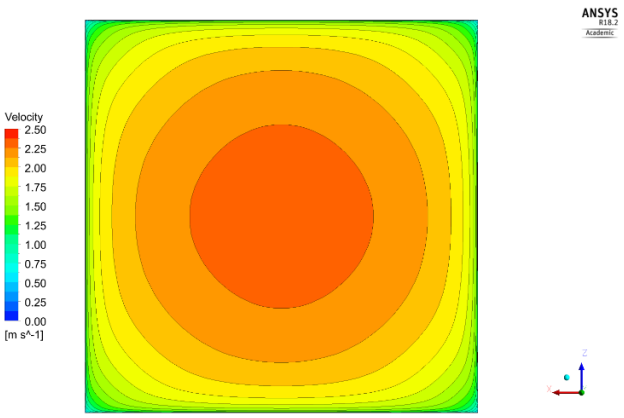

Fig. 7: axial velocity contour for square and 2m/s

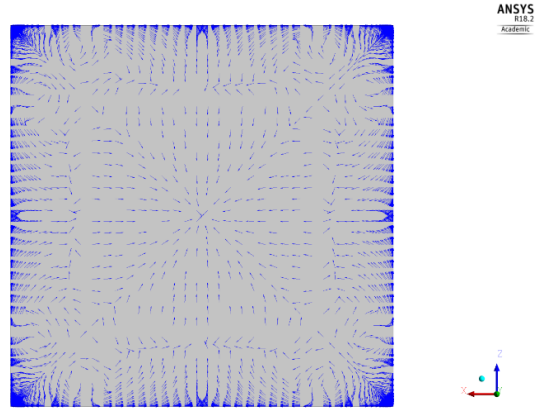

Fig. 8: secondary flow for square and 2m/s

The simulations were performed with ANSYS CFX 18. The mesh of the conduit is a manually generated structured hexahedral mesh. The inlet boundary comprises about 22500 hexahedral elements. Minimum and maximum angles were 90° and the maximum volume ratio were 1.2. The dimensionless wall distance (y+) is on average about 0.01 (for 0.2 m/s), 4 (for 2m/s) and 20 (for 10 m/s). The simulations were performed in steady state and with translational periodic boundary conditions. The solutions are based on the SST (shear stress transport) turbulence model. The calculations are solved with the high resolution advection scheme and automatic timescale. The RMS residuals were lower than 10^{-12}, the maximum residuals were at $1.1 \cdot 10^{-11}$, and the imbalance at $4.8 \cdot 10^{-12}$. The simulations required about 300 iterations to reach this convergence. The wall roughness was chosen as the one of sand/grain and set equal to 0.1mm For steel the corresponding value would be ten times smaller.

In Figure 9 the 3-dimensional plots of the normalized velocity profiles for the three velocities are shown. From these it seems that the shape of the profiles do not change much, especially for larger velocities. This can also be seen in the three area flow functions of Figure 10.

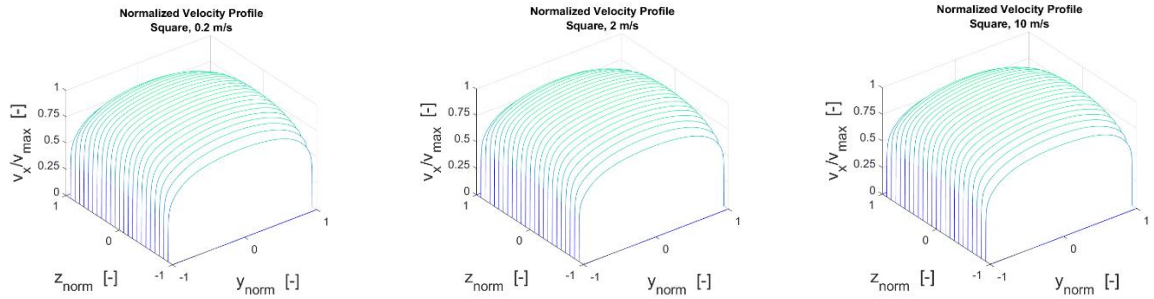

Fig. 9: normalized velocity profiles: left 0.2m/s, middle 2m/s, right 10m/s

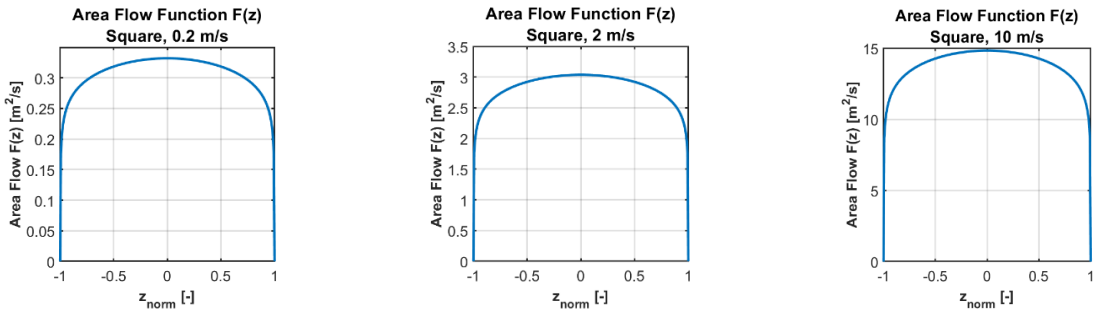

Fig. 10: Area flow functions (AFF): left 0.2m/s, middle 2m/s, right 10m/s

Figure 11 summarizes all the obtained relative error results. The following remarks can be added:

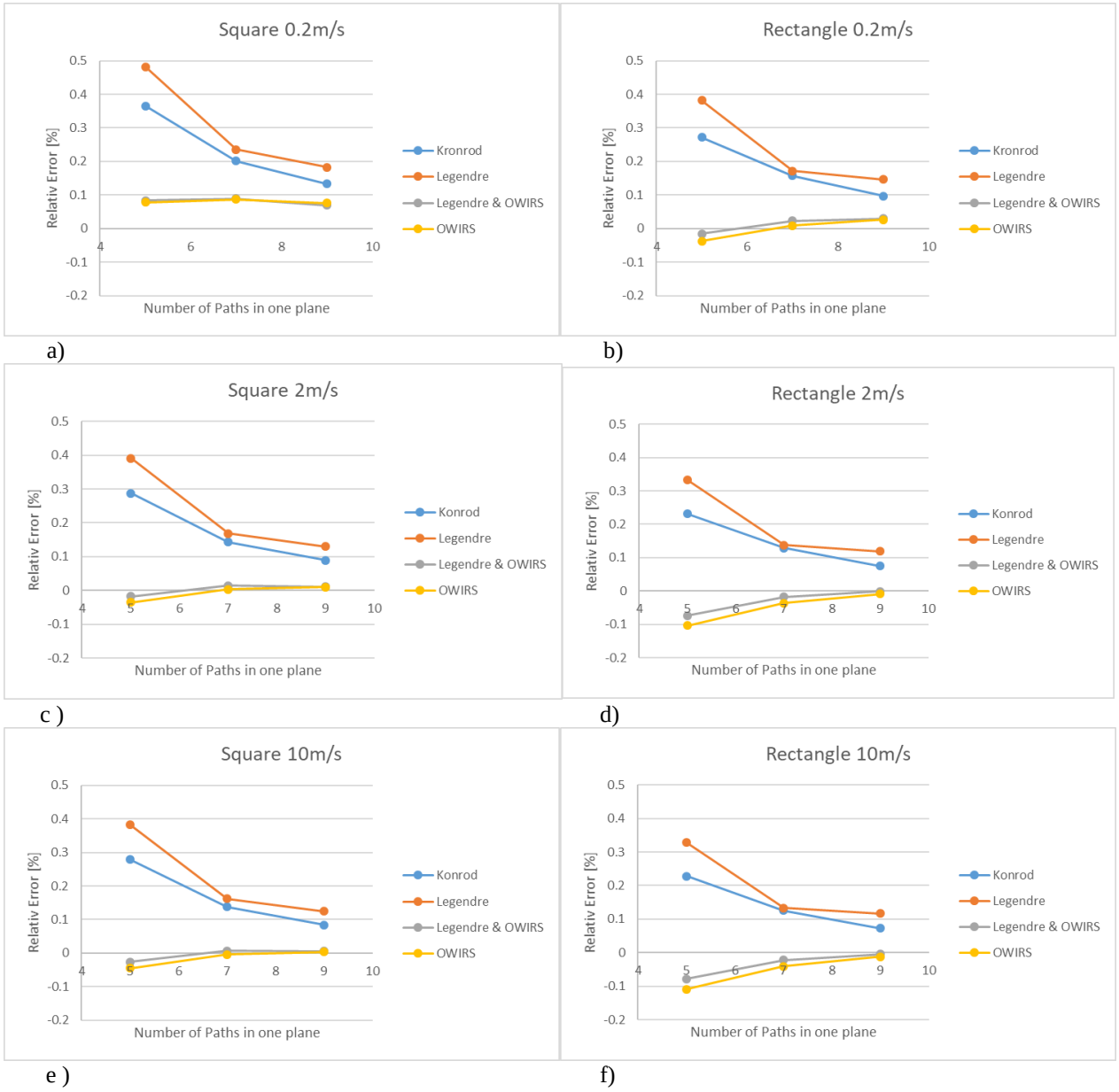

Fig. 11: Relative error curves for all simulated cases

- With increasing number of paths all error curves decrease strongly and slow down for higher number of paths.
- The Legendre positions & OWIRS case and the pure OWIRS case behave very similar and are clearly superior to the other two cases. Only in the case a): velocity of 0.2m/s and square cross section, the error is with ~0.1% for all path configurations constant and relatively high. For low velocities and square geometry, the velocity profile seems less to be of the OWIRS type as for higher velocities. For this situation it could be interesting to optimize the parameter κ as was suggested by Gruber & al [13].
- It is interesting to note that the Gauss-Kronrod case always performs better than the Gauss-Legendre case. To be specific, for N= 5 paths the improvement is ~0.1%,<~0.01% for N=7 and finally ~0,02% for N=9. The reason for the obtained type of decrease of improvement is not clear at the moment.

6. Conclusions

In situations, where the accuracy of the ATT multipath discharge measurement in rectangular conduits seems to be not reliable enough due to unknown or not removable adverse effects, the method of increasing the path number is a viable option. The strategy should be as follows:

- If all path positons can easily been shifted then an incremental increase from for instance 4 to 5 path with OWIRS positions and weights is for realistic cases the best choice.
- If all path positons can easily been shifted and in cases of a purely constant weighting function and multiplicative polynomial deviations the Gauss-Legendre is clearly the best method.

- If the old path positions cannot be moved, the Gauss-Kronrod procedure by interlacing new paths is in realistic cases most of the time better than all the other methods.
- For nonpolynomial and non OWIRS type of profiles (exponential, transcendental (see section 4.2), the Gauss-Kronrod seems to be a very good alternative, as it even outperforms other repositioned configurations with the same number of paths.

References

[1] A. S. Kronrod: Nodes and weights of quadrature formulas. Sixteen-place tables, New York 1965: Consultants Bureau (Authorized translation from the Russian)

[2] S. Marushchenko, P. Gruber: "Comparative Study of 4(8)-path and 5(10)-path configurations for ATT flow measurements in circular conduits", IGHEM 2014, Itajuba, Brasil

[3] IEC60041 norm: Field acceptance tests to determine the hydraulic performance of hydraulic turbines, storage pumps, storage pumps and pump-turbines, 1991

[4] ASME PTC-18 norm: Hydraulic turbines & pumps, 2016

[5] T. Staubli, P. Gruber, F. Fahrni: "Diagnosis of Acoustic Transit Time Data based on the Area Flow Function", IGHEM 2018, Beijing

[6] T. Tresch, B. Lüscher, T. Staubli, P. Gruber: "Presentation of optimized integration methods and weighting correction for the acoustic discharge measurement", IGHEM 2008, Milano

[7] B. Lüscher, T. Staubli, T. Tresch, P. Gruber: "Optimizing the acoustic discharge measurement for rectangular conduits", IGHEM 2008, Milano

[8] https://en.wikipedia.org/wiki/Gauss–Kronrod_quadrature_formula, cited June 2018

[9] S. E. Notaris: "Gauss-Kronrod Quadrature Formulae – Survey of Fifty Years of Research, *Electronic Transactions on Numerical Analysis*, vol. 45, pp. 371-404, 2016

[10] I. P. Mysovskih: "A special case of quadrature formulae containing preassigned nodes", (Russian), Vesci Acad. Navuk BSSR Ser. Fiz.-Techn. Navuk, 4 (1964), pp.125-127

[11] Arbeitsgruppe für laseroptische Strömungsdiagnostik, 2009

[12] Gersten, K., Herwig, G.: Strömungsmechanik. Grundlagen der Impuls-, Wärme- und Stoffübertragung aus asymptotischer Sicht. 1. Aufl., Vieweg-Verlag, Braunschweig Wiesbaden 1992.

[13] P. Gruber, T. Staubli, T. Tresch, F. Wermelinger: Optimization of the ADM by Adaptive Weighting for the Gaussian Quadrature Integration, IGHEM 2010, Roorkee, India